

RL-TR-95-282
In-House Report
January 1996



Optical Switch Evaluation

Joseph M. Osman

APPROVED FOR PUBLIC RELEASE; DISTRIBUTION UNLIMITED.

DTIC QUALITY INSPECTED 3

Rome Laboratory
Air Force Materiel Command
Rome, New York

19960508 211

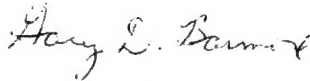
This report has been reviewed by the Rome Laboratory Public Affairs Office (PA) and is releasable to the National Technical Information Service (NTIS). At NTIS it will be releasable to the general public, including foreign nations.

RL-TR-95-282 has been reviewed and is approved for publication.

APPROVED: 

JAMES W. CUSACK, Chief
Photonics Division
Surveillance and Photonics Directorate

FOR THE COMMANDER:



GARY D. BARMORE, Major, USAF
Deputy Director
Surveillance and Photonics Directorate

If your address has changed or if you wish to be removed from the Rome Laboratory mailing list, or if the addressee is no longer employed by your organization, please notify RL (OCPA), Rome, NY 13441. This will assist us in maintaining a current mailing list.

Do not return copies of this report unless contractual obligations or notices on a specific document require that it be returned.

REPORT DOCUMENTATION PAGE			Form Approved OMB No. 0704-0188	
Public reporting burden for this collection of information is estimated to average 1 hour per response, including the time for reviewing instructions, searching existing data sources, gathering and maintaining the data needed, and completing and reviewing the collection of information. Send comments regarding this burden estimate or any other aspect of this collection of information, including suggestions for reducing this burden, to Washington Headquarters Services, Directorate for Information Operations and Reports, 1215 Jefferson Davis Highway, Suite 1204, Arlington, VA 22202-4302, and to the Office of Management and Budget, Paperwork Reduction Project (0704-0188), Washington, DC 20503.				
1. AGENCY USE ONLY (Leave Blank)	2. REPORT DATE January 1996	3. REPORT TYPE AND DATES COVERED In-House Aug 92 - Sep 93		
4. TITLE AND SUBTITLE OPTICAL SWITCH EVALUATION		5. FUNDING NUMBERS PE - 62702F PR - 4600 TA - P3 WU - 23		
6. AUTHOR(S) Joseph M. Osman				
7. PERFORMING ORGANIZATION NAME(S) AND ADDRESS(ES) Rome Laboratory (OCPA) 25 Electronic Pky Rome, NY 13441-4515		8. PERFORMING ORGANIZATION REPORT NUMBER RL-TR-95-282		
9. SPONSORING/MONITORING AGENCY NAME(S) AND ADDRESS(ES) Rome Laboratory (OCPA) 25 Electronic Pky Rome, NY 13441-4515		10. SPONSORING/MONITORING AGENCY REPORT NUMBER N/A		
11. SUPPLEMENTARY NOTES Rome Laboratory Project Engineer: Joseph M. Osman/OCPA (315)330-7671				
12a. DISTRIBUTION/AVAILABILITY STATEMENT Approved for public release, distribution unlimited.			12b. DISTRIBUTION CODE	
13. ABSTRACT (Maximum 200 words) We have evaluated nonlinear interface optical switches (NIOS) based on thin films of laser deposited metal oxide clusters. Films having nominal thickness $\approx 200\text{nm}$ and ranging in stoichiometry from $\text{WO}_{2.6}$ to $\text{WO}_{2.5}$, were evaluated in at least two configurations. Wanting to understand the considerable optical nonlinearity exhibited by these laser deposited group VI metal oxide cluster films, time resolved and other Raman experiments were conducted using WO_3 powder. In addition to helping explain the results of the NIOS testing, these and subsequent experiments revealed a phenomenon with considerable potential for optical switch, memory and other optical computing applications. Using this phenomenon, we conclude by discussing the viability of optical memory systems using the new media.				
14. SUBJECT TERMS optical memory, optical disk, optical computing, optical recording, optical switching, optical switches			15. NUMBER OF PAGES 32	
			16. PRICE CODE	
17. SECURITY CLASSIFICATION OF REPORT UNCLASSIFIED	18. SECURITY CLASSIFICATION OF THIS PAGE UNCLASSIFIED	19. SECURITY CLASSIFICATION OF ABSTRACT UNCLASSIFIED	20. LIMITATION OF ABSTRACT UNLIMITED	

TABLE OF CONTENTS

1. Nonlinear Interface Optical Switches	2
1.1. Introduction	2
1.2. WO_3 Time Resolved Photochromism Study	3
1.3. Future Plans	4
2. Photochromic All Optical Memory	6
2.1. Introduction	6
2.2. Discovery of Permanent Yellow to Blue Color Change	6
2.3. Erase and Cycling Study	7
2.3.1. Experimental Setup	7
2.3.2. Raman Spectroscopy	8
2.3.3. Read	9
2.3.4. Write	10
2.3.5. Erase	10
2.3.6. Conclusions	10
2.4. The Read Process	10
2.5. The Write Process	11
2.6. The Erase Process	12
2.7. System Issues	12
2.7.1. Erase and Write Time	12
2.7.2. Power for Write	12
2.7.3. Latency	13
2.7.4. Signal to Noise Ratio and Byte Error Rate	13
2.7.5. Lifetime	13
2.7.6. Cost Of Manufacture	14
2.8. Conclusions	14
2.9. Future Plans	14
3. Optically Written Electrically Read Memory	16
3.1. Introduction	16
3.2. Electrical Conductivity of WO_3 and Tungsten Bronzes	16
3.2.1. Band Structure	16
3.2.2. Resistivity of WO_3 Above Room Temperature	17
3.2.3. Resistivity of WO_3 Below Room Temperature	17
3.2.4. Electron Concentration from Hall Voltage Measurements	17
3.2.5. Hall Mobility of WO_3 Above Room Temperature	19
3.2.6. Small and Large Polarons	19
3.2.7. Conductivity of M_xWO_3 (Tungsten Bronzes)	20
3.2.8. Shear Planes in Substoichiometric WO_3	21
3.3. Conclusions	23
3.4. Future Plans for Page Memory	23
3.4.1. Thin Film Production	23
3.4.2. Resistance Measurements	23
3.4.3. Memory Element Design	23
3.4.4. Memory Element Test	23

1. Nonlinear Interface Optical Switches

1.1. Introduction

The Nonlinear Interface Optical Switch (NIOS) consists of 2 layers: one of an ordinary linear dielectric and a second thin nonlinear layer consisting of dielectric with an intensity dependent index of refraction, *i.e.*, an optical Kerr effect medium. This nonlinear layer has an index of refraction at weak input intensities which is slightly lower than the linear medium. When used for optical computer switching, all input beams are at or near the critical angle for total internal reflection (TIR). The beams are adjusted so that with no control beam or pulse, the data beam will undergo TIR, but when a control beam is present, the change in the nonlinear medium's index of refraction will lead to a transmission of the data beam through the interface. The transmitted beam gives C AND D, the reflected gives the EXCLUSIVE OR of C and D. These are sufficient to build a complete set of logic gates for a computer. When used for high power laser switching or eye/sensor protection, the device is structured such that light above a certain threshold causes the device to undergo TIR

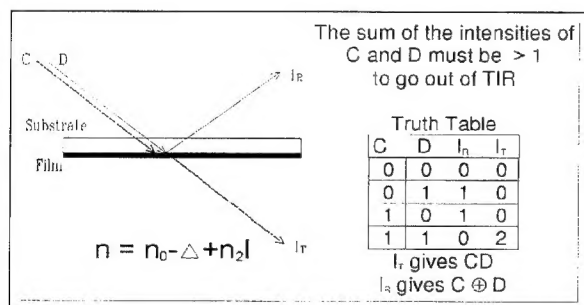


Figure 1. NIOS Schematic & Truth Table.

First proposed by Kaplan in 1977¹, they are currently under development at Penn State, where the nonlinear medium is a liquid crystal layer², the University of Iowa, where the nonlinear medium is an aqueous microparticle

suspension³, and BDM Corporation, which also uses microparticle suspensions⁴. The University of Iowa group has published suggested architectures for NI switches using two simple logic primitives : the Interaction gate with crossover and the Priesse gate with crossover. These are thermodynamically reversible gates⁵. The Iowa group has also made a study of enhancements to switching due to proper saturation of the nonlinear medium⁶. All these group's switches have large nonlinearities, but very low switching speeds.

In general, the major advantages of this type of switch over other types are that, because they do not use a resonator, they are capable of extremely fast response times if fast nonlinearities can be used, and if the nonlinearity itself is not a resonant nonlinearity, they can switch data signals of broad spectral bandwidth⁷.

The switches we are developing are made by Professor Joseph Chaiken of the Syracuse University Chemistry Department. They are made of nonstoichiometric tungsten trioxide cluster material. Tungsten oxides are tough refractory materials able to withstand high temperatures, and are familiar as the most common material used to make magnetron anodes. Bulk tungsten trioxide (WO_3) is a photorefractive material. We hope that the cluster material, by drastically decreasing the charge carrier travel distance, will speed up the nonlinear effect due to photorefraction, especially the recombination time.

The material is produced by pulsed laser fragmentation and deposition of fragments of an organometallic precursor in Prof. Chaiken's laboratory. By varying the wavelength, pulse duration, and gases present in the chamber, Prof. Chaiken can vary the stoichiometry much easier than previous groups making similar

materials, who commonly used high temperature sputtering.

The largest known nonlinearities available in a material system that can be integrable is in quantum confined semiconductors such as CdS in zeolites or semiconductor doped glasses. These nonlinearities are fast to switch on, but slow to switch off, because the matrix the semiconductor microcrystallites are in cannot be tailored for the fast carrier combination required. Nonstoichiometric cluster switches have the microcrystallites on the surface as a thin film, and Dr. Chaiken at SU has the capability of tailoring not only the microcrystallites, but also the matrix they are embedded in. The large nonlinearities mean changes will be easier to discern experimentally, making it easier to separate the effects of changes in switching.

Initial experiments on nonlinear interface optical switches are encouraging⁸, as the selected broad bandwidth media has strong nonlinearity.

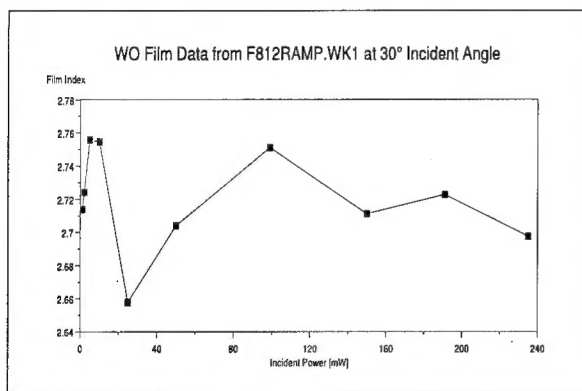


Figure 2. Film Index vs. Incident Power.

Now that we knew the film index from these results, we ordered ZnSe substrates to more closely match the film index.

1.2. WO₃ Time Resolved Photochromism Study

Bulk tungsten trioxide (WO₃) is of interest because it can be made to undergo reversible color changes, going from yellow to blue.

Tungsten oxides' proton mediated yellow to blue electrochromic transition has been studied for decades⁹, with use in optical displays in mind.

It is also photochromic. The exact mechanism involved that makes the material photochromic is still controversial¹⁰, and the speed of color change involved has not been measured.

After we had established the proper substrate to order, we decided to look at the speed of the yellow to blue transition in WO₃. We already had the proper setup from the film index measurements, and it looked like a quick but good paper. By looking at the change with our ultrafast pump-probe system, we hoped to be able to eliminate some mechanisms on time scale considerations. It would also give us a baseline to compare the switching speeds of the cluster material.

Later, by annealing cluster material and placing a proton donor layer next to it, we hoped to produce photochromic memory, which would be integrable with the switches. We had already proposed a ILIR/LDF effort to study this type of memory.

We were aligning the system to get a good spot on the material using the Nd:YAG laser, with a doubling crystal in line to produce 532 nm light. We were not using a harmonic separator to filter out the residual 1.06 μ m line. When we moved the spot across WO₃ powder sprinkled on a substrate, a blue line appeared and stayed. We repeated the write, and tried to estimate the

intensities of the 532 nm line and the 1.06 μm line.

Many groups have been working on tungsten trioxide, but as far as we know, none of them have been able to get a yellow to blue transition that was stable in atmospheric oxygen.

We never did measure the transition times, preferring to exploit our discovery by seeing if we could optically change the material back to yellow, thus erasing it. Then we would see if the material could be repeatably cycled through its transitions and thus act as an erasable optical memory.

1.3. Future Plans

After we are done developing WO_3 erasable memory systems, our test plan for the tungsten trioxide switches involves a cycle of testing for nonlinear switching behavior, changing the stoichiometry, and then retesting. As nonlinear switching behavior is observed, we will investigate how changes in the material change switching behavior.

A parallel experiment is to put the input beam through the substrate layer first, then the film (i.e. turn the switch over), rotate the switch until TIR just occurs, then increase intensity until a transmitted beam occurs. This latter configuration is also a nearly zero background measurement and in practice is less sensitive to photorefractive effects at the film-air interface. This will allow us to compare our results with published models¹¹. We could then use the results to determine the direction of changes in the material needed to optimize the Kerr coefficient.

Once the nonlinearity is optimized, then the switch can be evaluated in the typical pump

probe method in which a pulse of light is used to set up the nonlinearity and a later pulse, the probe/data arrives delayed to map out the switch transfer function.

Using a pump-probe system, we could determine the time parameters of nonlinear processes involved, then optimize the pulse length to produce best switching- low threshold energy with usable contrast and fanout.

We then should see if annealed cluster material will act as all optical erasable photochromic memory, which would be integrable with the switches.

After the material is optimized, we could investigate contrast enhancement due to soft saturation¹².

Later, we could integrate a simple logic primitive on a single substrate, either an Interaction gate with crossover or a Priesse gate with crossover¹³, and test the device for cascability, switching speed and switching energy.

- ¹. Kaplan, A.E., *Soviet Physics JETP*, Vol. 45, No. 5, pp. 896-905, May 1977.
- ². Khoo, I.C., *Applied Physics Letters*, Vol. 40, No. 8, pp. 645-647, 15 April 1982.
- ³. Cuykendall, R., and Strobl, K., *Journal of the Optical Society of America B*, Vol. 6, No. 5, pp. 877-883, May 1982.
- ⁴. Lawson, C.M., Euliss, G. W., and Michael, R.R., *Applied Physics Letters*, Vol. 58, No. 12, pp. 2195-2197, 20 May 1990.
- ⁵. Cuykendall, R., and Anderson, D.R., *Optical Communications*, Vol. 62, No. 4, pp. 232-236, 15 May 1987; Cuykendall, R., and Anderson, D.R., *Optics Letters*, Vol. 12, No. 7, pp. 542-544, July 1987; Cuykendall, R., *Applied Optics*, Vol. 27, No. 9, pp. 1772-1779, 1 May 1988; Cuykendall, R., and Strobl, K., *Journal of the Optical Society of America B*, Vol. 6, No. 5, pp. 877-883, May 1989; Strobl, K., and Cuykendall, R., *Applied Optics*, Vol. 29, No. 2, pp. 187-194, 10 January 1990.
- ⁶. Strobl, K. H., and Cuykendall, R., *Physics Review A*, Vol. 40, No. 9, pp. 5143-5146, 1 Nov 1989; Cuykendall, R., and Strobl, K.H., *Physics Review A*, Vol. 41, No. 1, pp. 352-358, 1 January 1990; Strobl, K. H., and Cuykendall, R., *Optics Letters*, Vol. 15, No. 2, pp. 96-98, 15 January 1990; Strobl, K. H., and Cuykendall, R., *Optical Communications*, Vol. 74, No. 6, pp. 389-392, 15 January 1990.
- ⁷. Smith, P.W., *et al.*, *IEEE Journal of Quantum Electronics*, Vol. QE-17, No. 3, pp. 340-348, March 1981.
- ⁸. Osman, J.M., and DeVaul, B., *High Speed Laser Facility*, RL TR-95-136.
- ⁹. Dautremont-Smith, W.C., *Displays*, 3-22, January 1982.
- ¹⁰. Gabrusenoks, J.V., *et al.*, *Solid State Ionics*, Vol. 14, pp. 25-30, 1984.
- ¹¹. Khoo, I. C., and Zhou, Ping, *Journal of the Optical Society of America B*, Vol. 6, No. 5, pp. 884-888, May 1989; Anderson, D. R., and Regan, J.R., *Journal of the Optical Society of America A*, Vol. 6, No. 9, pp. 1484-1492, September 1989.
- ¹². Strobl, K. H., and Cuykendall, R., *Physics Review A*, Vol. 40, No. 9, pp. 5143-5146, 1 Nov 1989; Cuykendall, R., and Strobl, K.H., *Physics Review A*, Vol. 41, No. 1, pp. 352-358, 1 January 1990; Strobl, K. H., and Cuykendall, R., *Optics Letters*, Vol. 15, No. 2, pp. 96-98, 15 January 1990; Strobl, K. H., and Cuykendall, R., *Optical Communications*, Vol. 74, No. 6, pp. 389-392, 15 January 1990.
- ¹³. Cuykendall, R. and Anderson, D.R., *Optical Communications*, Vol. 62, No. 4, pp. 232-236, 15 May 1987.

2. Photochromic All Optical Memory

2.1. Introduction

Systems requirements for projected future AF radar and intelligence signal processing systems include large capacity, high speed memory storage. The use of optics provides both significant speed and storage advantages over electronic approaches. Optical transitions can be very fast, and the massively parallel nature of optical systems can provide for high density information storage.

We have developed a new and highly promising optical memory technology based on tungsten oxide. The basic discovery at the heart of the system has not yet been published, but promises to impact optical memory systems substantially. Initial military and civilian exploitation will probably be for use as a disk memory system, since it is easily integrable into current disk systems. We are currently targeting our efforts toward producing photochromic optical memory media for optical disks.

We have discovered that using two different wavelengths of light, one blue-green and one infrared (IR), we can cause tungsten oxide (WO_3) to permanently change color (write) from yellow to blue. We have also discovered how to reverse the process (erase) using a single IR wavelength of light.

It has been known for some time that WO_3 and some other transition metal oxides can undergo color changes due to incident light. This process is called photochromism. It has also been known that WO_3 and some other transition metal oxides form mixed valence compounds when so colored. Some examples are WO_3 , V_2O_5 , TiO and MoO_3 .

In the case of WO_3 , the erased material contains only the W^{6+} oxidation state, while the written material contains both W^{6+} and W^{5+} oxidation states. Previously, the compound would only undergo a photoinduced color change if oxygen was removed from its surface, either by enclosing it with an inert gas atmosphere or a vacuum. Upon reintroduction of atmosphere, the material would erase.

2.2. Discovery of Permanent Yellow to Blue Color Change

As related in Section 1.2, we were planning on measuring the speed of the yellow to blue transition in WO_3 . We were aligning the system to get a good spot on the material using the Nd:YAG laser, with a doubling crystal in line to produce 532 nm light. We were not using a harmonic separator to filter out the residual 1.06 μm line. When we moved the spot across WO_3 powder sprinkled on a substrate, a blue line appeared and stayed. We repeated the write, and estimated the intensity of the 532 nm line as about 50 mW and the 1.06 μm line as about 0.5 W. We estimated both had about a 300 μm spot size.

We decided that the most likely reason the 1.06 micron light made the transition permanent was that it was heating the lattice and allowing it to restructure in the blue form before an atmospheric oxygen could be taken in by the material. By heating the blue form in atmospheric oxygen either by using 1.06 micron light only or by heating the material in an oven, we might be able to erase it. It was also important to determine if there was any limitation on cycling, i.e., if the material did not completely return to one state from the other. For these reasons we set up a more precise system for further study.

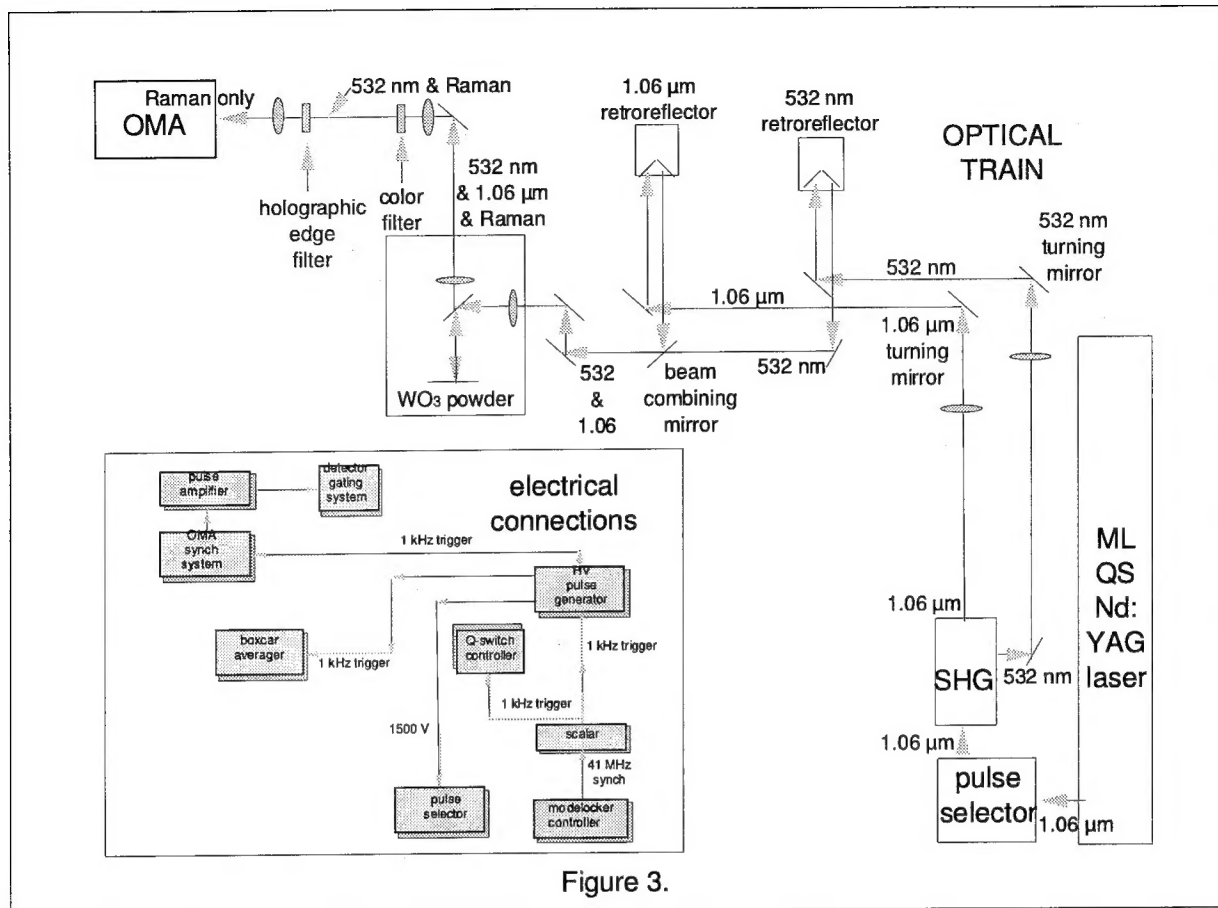


Figure 3.

2.3. Erase and Cycling Study

2.3.1. Experimental Setup

Figure 3 shows our experimental setup. The laser was modelocked and Q-switched such that every millisecond we illuminated the sample with a 200 ns Q-switched pulse envelope consisting of about a dozen 140 ps pulses 12 ns from each other. This lead to a low duty cycle for the experiment of

$$\frac{(12)(140 \times 10^{-12})}{1 \times 10^{-3}} = 1.68 \times 10^{-6}$$

As will be explained later, the detection system also had a low duty cycle. In practice, there will be no need for anything other than CW lasers to write, erase and read this type of memory. This setup was designed principally for time resolved spectroscopy to further study

the mechanisms involve in writing and erasing, not to act as a system testbed.

The pulse selector is in the optical path to allow us to pick out a single pulse from the Q-switched pulse enveloped for time resolved experiments. We were not using it for single pulse selection, instead, we adjusted it to pass the entire envelope.

The second harmonic generator (SHG) converted about 10% of the 1.06 μm light into 532 nm light, without lengthening the pulse duration. The harmonic separator in the SHG split the SHG output such that most of the 1.06 μm light passed through while most of the 532 nm light was reflected into a separate beam. In order to further filter the beams, the nominally 1.06 μm beam is passed through a specific 1.06 μm interference filter. Also, specific 1.06 μm

quarter-wave stack mirrors were used where possible to further filter out the 532 nm light. A similar arrangement was used to filter the nominally 532 nm beam.

The output from an Antel S-2 silicon detector, which had a 25 ps rise time, was input into a Tektronix S-4 Sampling Head. The S-4 Sampling Head had a 35 ps rise time. The S-4 was in an EG&G Boxcar Amplifier. In this way we were able to simultaneously detect both color pulses at the WO_3 sample and adjust the retroreflectors so that both wavelength pulses arrived simultaneously on the sample.

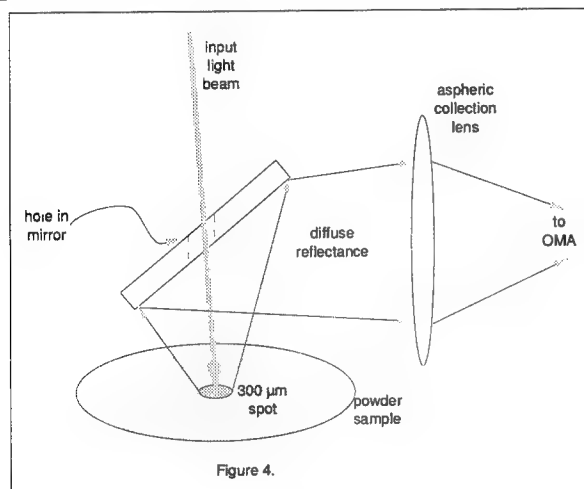


Figure 4 shows the diffuse reflectance setup inside the light tight box. The spatially and temporally collimated beams were focused by a single lens, went down through a hole drilled in a 45° mirror and illuminated the sample. The spot size on the sample was about 300 μm .

The sample itself consisted of 99.995% pure WO_3 powder, which was pressed into circular depressions in a 2 cm diameter fused quartz substrate. The substrate was about 0.25 cm thick, with the depressions having a depth about 1/3 that of the substrate.

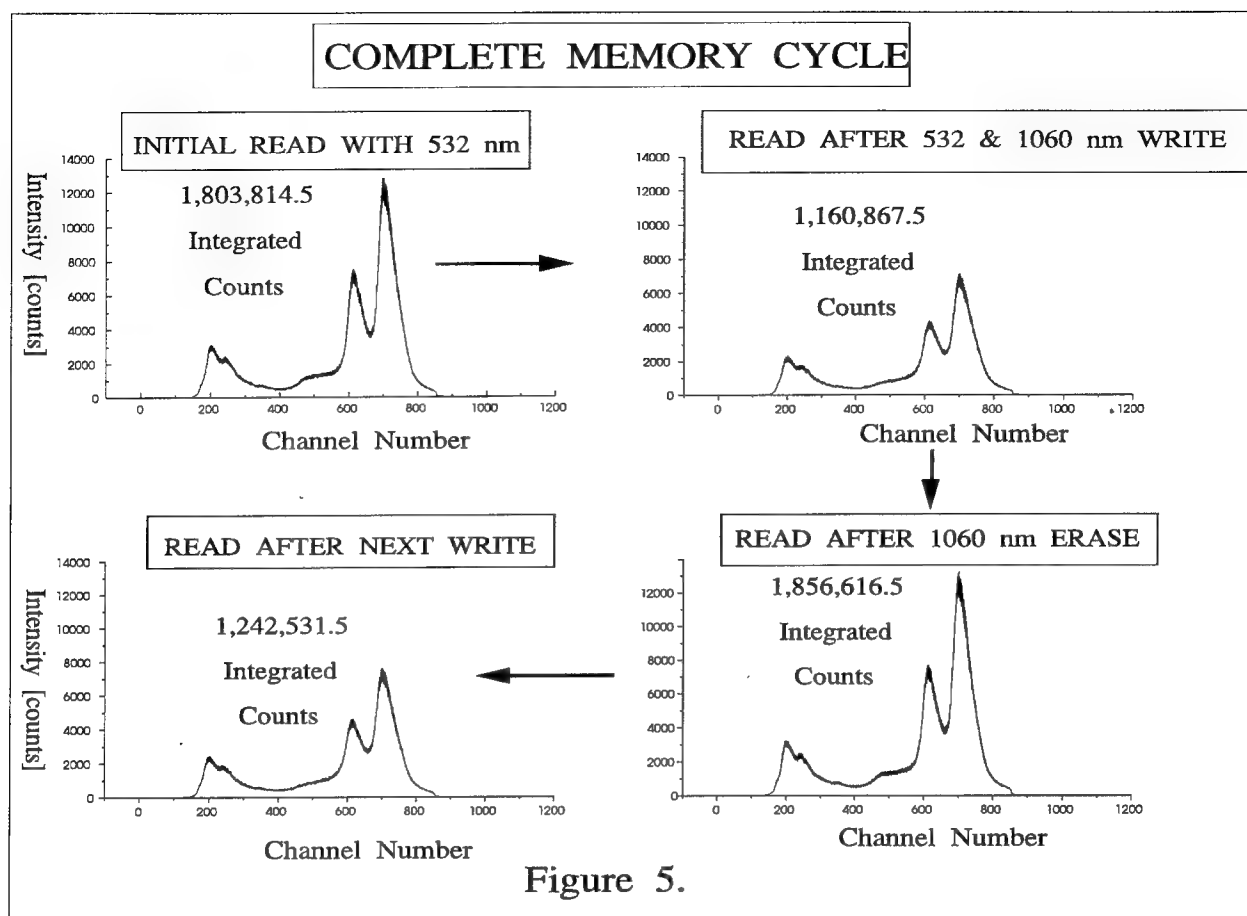
About 20% of the diffuse reflected light was steered by the 45° mirror through a strong

collection lens into the second 45° collection mirror. After this, a color filter removed most of the 1.06 μm light. It then went through a holographic edge filter that Physical Optics Corporation had loaned us. The holographic edge filter filtered out the incident 532 nm light (called the Rayleigh line in Raman spectroscopy), and allowed the nearby 555 nm Raman feature light through. A cylindrical lens imaged the Raman light into the entrance slit of an Instruments SA 0.32 meter Czerny-Turner monochromator which contained a 1200 grooves/mm grating. The light from the grating was internally imaged onto the monochromator exit slit. There it entered a 1024 channel linear photodiode array. This array was part of an EG&G PARC OMA III optical multichannel analyzer system.

The output of this system was a plot of counts versus channel number as seen in figure 5. The number of counts was proportional to intensity, while the channel number was proportional to wavelength. The tail of the 532 nm Rayleigh line was at about channel number 200, while the highest intensity Raman feature was at about 555 nm.

2.3.2. Raman Spectroscopy

Interaction between the incident light and bound electrons in the sample results in a scattering process because the time varying field of the light induces a dipole moment, M , in the sample.¹⁴ The induced moment varies with the frequency of the incident light and generates Rayleigh scattering at the same frequency, and hence wavelength, as the incident light. A Raman feature is an inelastic scattering event which occurs with a much lower probability when energy is removed from the oscillating material by a vibrational excitation (phonon) in the material. This is termed a Stokes process, and the scattered light



is lower in energy, and hence higher in wavelength, than the incident light. Anti-Stokes processes are where the scattered light gains energy from a material phonon and thus create scattered light lower in wavelength than the incident light. We looked at the Stokes features in our experiment.

We had been planning to use Raman spectroscopy in our time resolved photochromism study of WO_3 because the yellow state has strong Raman features that are lacking in the blue state. In the case of WO_3 , There is a W-O scissors mode at 716 cm^{-1} (channel number 620 in Figure 5) and another W-O scissors mode at 805 cm^{-1} (channel number 720 in Figure 5).

We gated our Optical Multichannel Analyzer (OMA) to count for 100 ns starting 25 ns after

it was triggered. In this way we preferentially counted the Raman signal, without counting a lot of background for the remaining part of the millisecond until the next pulse. This added another low duty cycle to the experiment, but because it was simultaneously triggered, it overlapped the original in time.

2.3.3. Read

The upper left hand plot of Figure 5 shows a Raman read of previously unwritten yellow WO_3 powder. The 3 other plots are also Raman reads. These reads were for 100 s, which due to our low duty cycle, meant the sample was irradiated with green light for only 0.168 ms. The Raman signal is at least 1/100 that of the reflected signal, and our collection optics brought less than 10% into the detector, giving

a rough estimate of about $0.3\ \mu\text{s}$ to read the non-Raman reflected signal.

2.3.4. Write

Simultaneously presented YAG laser beams at 1.06 microns and (doubled YAG) at 532 nanometer were used to write bits on the powder. As shown on the upper right hand plot of Figure 5, the Raman intensity is halved. This may be because the W^{5+} and W^{6+} oxidation states are present in about equal numbers. Alternatively, the write beam may have only changed the material in its central maximum area. The read beam was the same diameter as the write beam, so it may have been reading the outer unwritten area.

The first read was purposely long to determine how low the written signal would go. It was erased for 21 minutes, which meant that with our low duty cycle, both colors of light were on the material for 2.12 ms.

The second read after write of this particular cycle, shown in the bottom left hand plot, gave a slightly larger integrated intensity, but this was within statistical uncertainty for the process, as later cycles on the same spot showed. It was after a 5 minute, or 0.504 ms with our duty cycle, write.

Our large spot size ($300\ \mu\text{m}$) has an area 9×10^4 larger than a $1\ \mu\text{m}$ spot size. Our write and erase times should decrease dramatically when we start putting the same amount of power into micron size spots.

2.3.5. Erase

Erase was accomplished using the 1.06 micron beam alone. It is shown in the bottom right hand plot of Figure 5. What is most important is that there is no degradation of signal from

the original previously unwritten state. This particular erase was 7 minutes (0.706 ms).

2.3.6. Conclusions

This experiment proved that we can completely cycle the memory material. We took long exposures to ensure that the material would be driven to its limits. No attempt was made to optimize any parameter for speed.

2.4. The Read Process

In our experiment, we used Raman to read the state of our material. Using reflectance should give more than 100 times the signal. Absorption and scattering might give significant signal in transmittance through thin films on clear substrates. The main caveat for optical read is that the read beam not be intense enough to write or damage the material or the substrate. A third color could be used to take advantage of reflectance maxima. If Raman is used to read, the third color could be the wavelength of maximum resonance enhancement. This could lead to a smaller head if the write laser wavelengths were picked for material absorption maxima, in order to reduce their power requirements. In order to reduce the area per bit, the shorter wavelengths are preferable.

As section 3 of this report will show, the electrical properties of the two states are different. This can be used to make an optically addressed electrically read memory.

2.5. The Write Process

WO₃ has a distorted version of the ReO₃ structure (figure 6a), which is a simple cubic lattice of tungsten with each tungsten atom the center of a WO₆ octahedron.

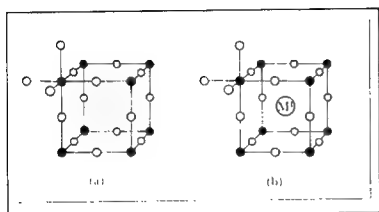


Figure 6. (a) ReO₃ structure; (b) Perovskite-like tungsten bronze structure. Filled circles are W⁶⁺, open circles are O²⁻, M¹ is a metal ion¹⁵.

Figure 7 shows a more accurate representation of the WO₃ structure.

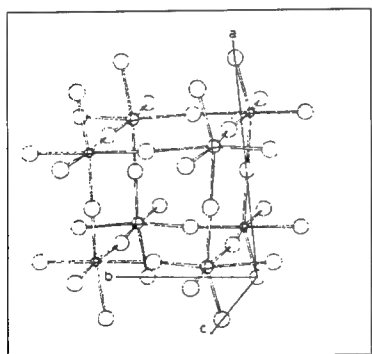


Figure 7. WO₃ structure¹⁶.

The internal vibrations of the octahedral units, including a W-O scissors mode at 716 cm⁻¹ (channel number 620 in Figure 5) and another W-O scissors mode at 805 cm⁻¹ (channel number 720 in Figure 5), are what we saw in our Raman experiment.

When small amounts of metals (M), usually hydrogen or sodium, are added to WO₃, a tungsten bronze MWO₃ is formed. The WO₃ lattice restructures with a proton or a positive metal ion in the center of the simple cubic tungsten lattice (figure 6b). This restructuring

also causes a color change from yellow to blue, and a change in Raman features.

In our new process, the 532 nm radiation excites electrons, principally from the oxygens, which are trapped by W⁶⁺ metal ions at the center of the octahedra, thereby forming W⁵⁺ ions. This should occur on a time scale of a picosecond or less, since the corresponding lengths in the compounds are so short. The material is now in the mixed valence blue colored state. The fact that color changes occur due to the formation of mixed valence compounds has been known since early in this century¹⁷, and soon after, it was learned that mixed valence compounds show an increase in electrical conductivity¹⁸.

The shift is made permanent by the heating effect of the 1.06 micron beam which drives out bonded oxygen.

The final result is the chemical reaction



which is permanent until the material is reheated to a temperature greater than 400°

It has been known for years that heating WO₃ in a vacuum causes the formation of substoichiometric WO_{3-x}, with x being a small number, through the formation of crystallographic shear planes. Upon heating, the oxygen vacancies all line up along a crystallographic axis, the lattice shears, and octahedra along the shear plane then share edges, instead of being corner sharing as is seen in Figure 8. This results in removing some oxygen atoms. This is explained in greater detail in section 3.2.8.

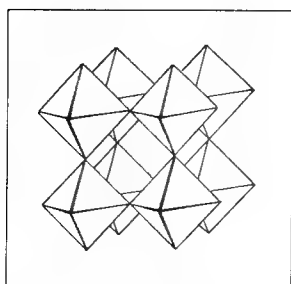


Figure 8. MO₆ octahedra stacking¹⁹.

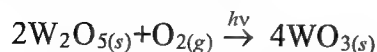
The structure of W₂O₅ is such that all octahedra share edges, not just a few percent, as in substoichiometric WO_{3-x}. The electron excitation and W⁵⁺ ion formation must be causing further weakening of W-O bonds, as can be seen by the reduction of the W-O scissors modes we see in the Raman plots. If so, the loosened oxygen atoms may form O₂ and leave the material, leading to total edge sharing, and the formation of a new stable structure.

Since the low power of 532 nm we used did not write the material by itself, the heating effect of the 1.06 micron light is also needed to heat and soften the lattice giving greater mobility to both electrons and ions.

2.6. The Erase Process

WO₃ is the thermodynamic ground state for the tungsten-oxygen system, and an erasure from W₂O₅ to WO₃ is possible using heat alone.

When we erase using IR alone, the material absorbs the IR and is heated. Since the material is surrounded by ambient air, there are plenty of oxygen atoms striking the surface to take place in the chemical reaction



which is permanent until the material is written again.

A global erase of an entire disk can be performed by placing the entire disk in an oven or tube furnace for a minute or two.

2.7. System Issues

We also made an attempt to model some possible system characteristics using our evaluation data and compare our possible system with current erasable optical memory systems.

2.7.1. Erase and Write Time

ERASE AND WRITE TIME	
WO ₃	¾ 0.144 ms in 120 s
WO ₃ (modeled)	¾ 0.144 ms
Magneto-optical	167 ms

The modeled WO₃ time does not include any speed increase due to packing the laser's power into a smaller spot size. The magneto-optical time is for a sector erase. Because of the need for a single large magnet for writing and erasing, the magneto-optical system can only erase or write an entire full revolution sector at a time. Single bit write for magneto-optical media is 100 ns at power levels of 30 to 40 mW²⁰.

2.7.2. Power for Write

POWER FOR WRITE	
WO ₃	¾ 300 mW / 7 x 10 ⁵
WO ₃ (modeled)	¾ 0.334 μW / 0.78 μm ²
Magneto-optical	8 mW / 0.78 μm ²

For this comparison, the experimental laser power was averaged over its 300 μm area. Writing at faster speeds will probably require more laser power. What is exciting is that at these low powers, we can start using Vertical Cavity Surface Emitting Lasers (VCSELs) which are much more compact and have more

circular and less astigmatic beams than the more common edge-emitting laser diodes.

2.7.3. Latency

READ TIME (latency)	
WO ₃	¾ 0.122 ms in 100 s OMA
WO ₃ (modeled)	¾ 1 ms
Magneto-optical	33 ms

Because of the smaller heads possible due to lower power requirements and lack of a magnet in the head, it should be possible to go to multiple heads per platter side. If these are placed equidistant on a rigid bar, the single head latency can be divided by the number of heads. The above assumes a 40 laser head (32 data and 8 checksum bits). The same rotational speed is assumed. If individual bits can be written faster, the disk speed can be increased, decreasing the latency even more.

2.7.4. Signal to Noise Ratio and Byte Error Rate

Current magneto-optical disks require that the differential detector be capable of determining whether a highly polarized input beam is shifted less than 0.6 degrees in polarization, with the direction of shift determining whether the bit is a one or a zero. This leads to a very poor signal to noise ratio for magneto-optical disks. What is even more of a problem is that the material has micron size pits, both upon manufacture and with aging. Typical disks initially have about 15% of their area that is too pitted for use. The disk must be read and a lookup table of bad areas produced. Every sector that is written must be read and compared with the sector still in electronic memory. If any other dropouts are found, the look up table must be updated, and the sector rewritten.

Phase change disks use the difference in reflectance between crystalline and amorphous areas of the same material. Tellurium suboxide, for example, has 26% reflectance in the amorphous state and 18% reflectance in the microcrystalline state²¹.

We got a contrast ratio of 1.5:1 for our Raman reads. The contrast in reflectance between our pale yellow and dark blue should be much greater than phase change can achieve.

The best way of determining our byte error rate will be to hook a bit error rate tester (BERT) into our system.

We only measured 4 written peaks in our experiment, which is not enough to be statistically significant. Later studies should be continued long enough to achieve a statistically significant sample size. Then we could compute a signal to noise ratio (SNR).

One quick estimation²² of bit error rate uses an SNR defined as the ratio of the mean square of the signal current to the sum of the mean square fluctuations of the currents. Q is one half of the SNR. Then

$$BER1 = \frac{1}{2} \text{erfc}(Q),$$

where erf is the Gaussian error function and erfc is the complimentary error function.

Another estimation²³ is

$$BER2 = \frac{1}{\sqrt{2\pi Q^2}} \exp\left(-\frac{Q^2}{2}\right)$$

2.7.5. Lifetime

LIFETIME	
WO ₃ (measured)	
WO ₃ (modeled)	as good or better
Magneto-optical	10 ⁶ -10 ⁷ cycles

As mentioned previously, the magneto-optic media suffers from dropouts. Phase change media suffers from fatigue over many cycles, and has a lower cycle lifetime than magneto-optical. The lifetime of our media will depend on material adhesion to the surface and cycle fatigue also. More long time/multicycle studies are needed.

2.7.6. Cost Of Manufacture

The low yield of magneto-optical disk manufacture due to the dropout problem and the use of rare earths (about 25%) in the media leads to expensive disks.

The commercial market for both WORM and erasable disks has not increased anywhere near the manufacturers' hopes. This is principally because the costs of making the media have not dropped. The main reason phase change media is being sold commercially, despite its limited cycle lifetime, is because of its lower media cost.

Tungsten oxide is cheap. 99.99% pure tungsten oxide is \$103.00 for 250 g. 99.8% pure is \$224.00 for 2 kg²⁴. A thin film thickness of about 200 nm is all that is needed, which means that 250 g or 2 kg will make a lot of disks.

2.8. Conclusions

We have invented an erasable optical memory suitable for optical disc systems. This new all

optical memory is much faster, requires μW rather than mW , and will be cheaper to manufacture than magneto-optical (MO) memory. The increased speed, simplicity, and accuracy of this new memory, coupled with its ability to work with blue or even shorter wavelength lasers, means that it is a candidate to replace current magnetic hard/floppy disks as well as MO disks. Multiple heads will be cheaper and easier as well, due to the all optical polarization insensitive nature of system and low write and read power requirements. The tungsten oxide technology is compatible with blue laser diodes which improve storage density. Hence it is expected that this invention will result in dramatically improved optical storage systems. A journal paper is in preparation, and an invention disclosure has been submitted.

2.9. Future Plans

We plan to exploit our invention of a new optical memory system by the following:

1. Fabrication of disks and chemical evaluation at Laser Chemical Corporation.
2. System evaluation at Photonics Center.
3. Determine optimum power and wavelengths of light for each form of media.
4. Determine smallest possible bit area for each type of media.
5. Determine role of humidity and absorbed water.
6. Use results to modify disk fabrication for a better system.
7. Demonstrate invention to potential investors or licensees.

- ¹⁴Exarhos, Gregory J., "Raman Spectroscopy of Thin Films", in Hummel, Rolf E., and Guenther, Karl H., eds., *Handbook of Optical Properties Vol. 1: Thin Films for Optical Coatings*, CRC Press, 1995.
- ¹⁵Duffy, J.A., *Bonding, Energy Levels and Bands in Inorganic Solids*, p. 185, Longman, 1990.
- ¹⁶Salje, E., *Acta Cryst.*, **B33**, 574-577, (1977)
- ¹⁷Hofmann, K.A., and Hoeschele, K., *Ber. Deut. Chem. Ges.*, **48**, 20, (1915)
- ¹⁸Wells, H.L., *Am. J. Sci.*, **3**, 417, (1922).
- ¹⁹Cox, P.A., *Transition Metal Oxides*, p. 22, Clarendon Press, Oxford, 1992.
- ²⁰Balasubramanian, K., "Thin Film Media for Optical Data Storage", in Hummel, Rolf E., and Guenther, Karl H., eds., *Handbook of Optical Properties Vol. 1: Thin Films for Optical Coatings*, CRC Press, 1995.
- ²¹Marchant, Alan B., *Optical Recording*, p. 45, Addison-Wesley, 1990.
- ²²Cheo, Peter K., *Fiber Optics Devices and Systems*, p. 266, Prentice Hall, 1985.
- ²³Cheo, Peter K., *Fiber Optics and Optoelectronics*, p. 394, Prentice Hall, 1990.
- ²⁴Alfa/Aesar 1995-1996 Catalog, p. 551.

3. Optically Written Electrically Read Memory

3.1. Introduction

Our recently developed tungsten oxide optical memory, as well as other all optical memories, have the capability of producing dense two dimensional patterns of binary light beams as their output. Current methods of reading these patterns perform digital light to analog electrical conversion using arrays of CCDs or detectors. The information is then sequentially read out row by row, thresholded, and transported through wires or striplines into an electronic memory. We should develop a system to place the dense array of information directly into an electronic memory, simplifying the process as well as lowering the chip real estate needed for the task.

For this purpose, we should develop a two-dimensional optically addressable, electrically readable binary page memory. For this effort we must know the electrical properties, especially the electrical conductivity, of our new optical memory media. If its electrical properties differ enough in its two states, it should be tested for electrical readability.

3.2. Electrical Conductivity of WO_3 and Tungsten Bronzes.

3.2.1. Band Structure

In WO_3 , the $\text{Mg}^+/\text{Mg}^{2+}$ of Figure 9 is replaced mostly by $\text{W}^{6+}(5d)$ orbitals. The Madelung potential is an electrostatic potential acting on an electron due to the ionicity of the lattice. The polarization is the polarization the electron causes in the nearby lattice. The overlap is the broadening of electronic levels due to the spatial overlap between ions.

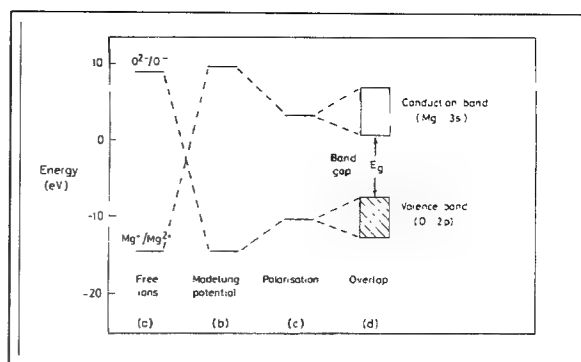


Figure 9. Ionic-model of the band gap in MgO ²⁵.

WO_3 is more complex than the simple picture of Figure 9 for MgO . In WO_3 , since the $\text{O}^{2-}(2p)$ orbitals are lower in energy than the $\text{W}^{6+}(5d)$ orbitals, the empty valence band is formed from a bonding combination of the $\text{O}^{2-}(2p)$ orbitals and mostly the $\text{W}^{6+}(5d)$ orbital. Similarly, the conduction band is formed from an antibonding combination of the $\text{O}^{2-}(2p)$ orbitals and mostly the $\text{W}^{6+}(5d)$ orbital.

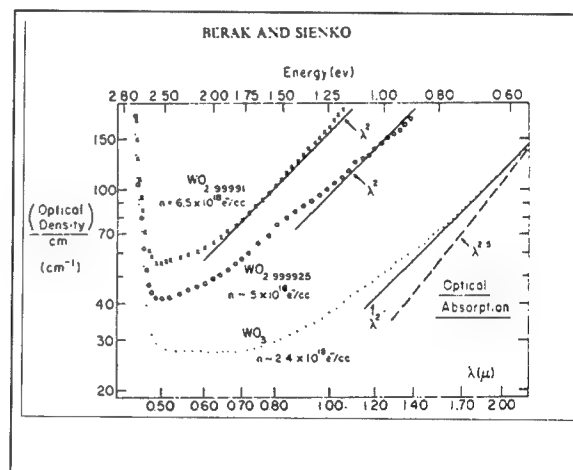


Figure 10. Optical absorption vs. wavelength for 3 crystals varying in W/O ratio ²⁶.

The band gap, E_g , is about 2.7 eV for WO_3 . This is a small energy compared to the much larger effects shown in Figure 1. The band gap can not yet be accurately calculated from the spectroscopic levels, then applying the Madelung potential and so on. It must be measured, as it was for Figure 10, which shows the allowed transition of electrons from the top

of the filled band to the bottom of the empty band.

Although WO_3 has a small semiconductor-like band gap, many other transition metal oxides end up with a wider gap, and thus are insulators, or have overlap between the valence and conduction bands, and thus are metallic.

3.2.2. Resistivity of WO_3 Above Room Temperature

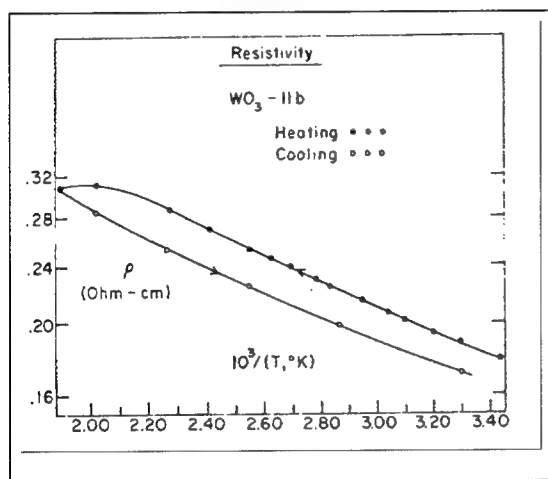


Figure 11. Logarithm of the resistivity of a WO_3 crystal vs. reciprocal temperature above room temperature ²⁶.

Figure 11 shows insulator or semiconductor type behavior of the resistivity of WO_3 . The hysteresis is due to an increase in carrier concentration, probably caused by the diffusion of gallium wetting agent into the crystal at high temperature ²⁶.

3.2.3. Resistivity of WO_3 Below Room Temperature

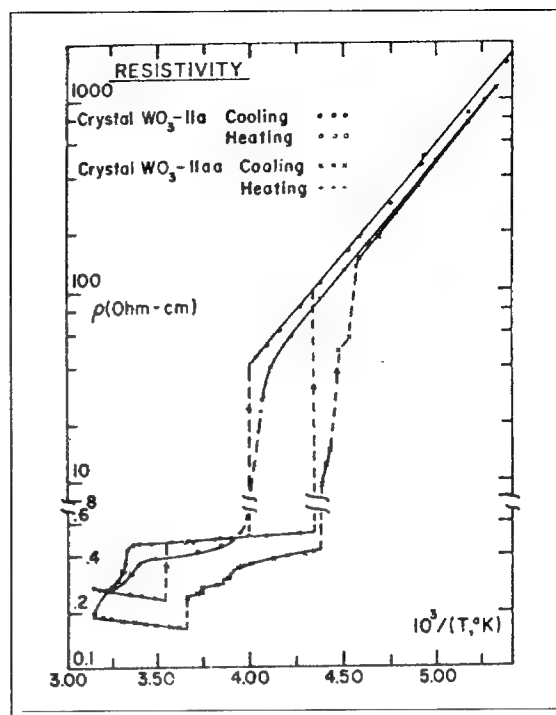


Figure 12. Logarithm of the resistivity of WO_3 crystals vs. reciprocal temperature below room temperature ²⁶.

The discontinuities in Figure 12 are due to a triclinic phase transition at -43°C and a triclinic to monoclinic phase transition at 9°C . Crystal IIaa is twinned. In twinned crystals, different domains transition at different temperatures. That is why the transitions are not as sharp for the twinned crystal.

3.2.4. Electron Concentration from Hall Voltage Measurements

Figures 13 and 14 show the electron concentration as determined by Hall voltage measurements.

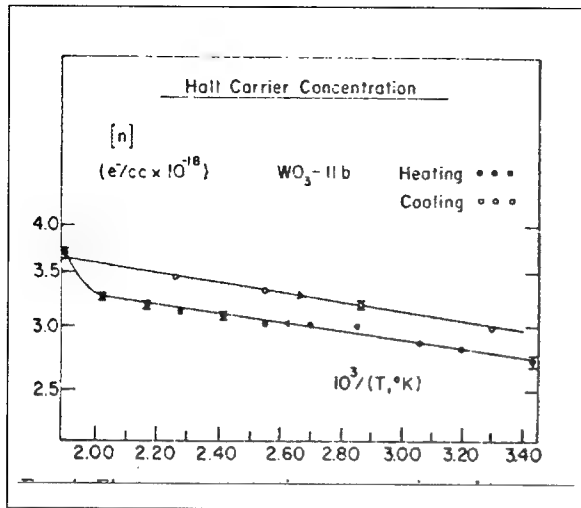


Figure 13. Electron concentration vs. $1/T$ for a WO_3 crystal above room temperature²⁶.

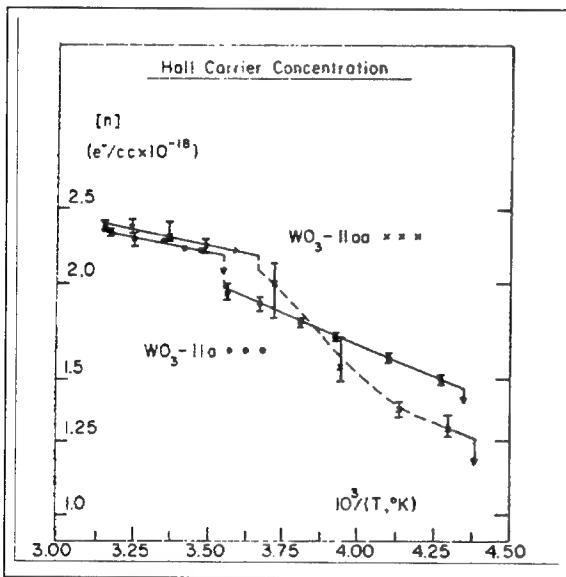


Figure 14. Electron concentration versus $1/T$ for WO_3 crystals below room temperature²⁶.

For these, the equation $R_H = rB/Nq$ was used, where both the scattering mechanism constant r and the band shape parameter B were assumed equal to unity at all temperatures. This gives $R_H = 1/nq$, which means Figure 13 and 14 can be compared to Figure 15, which is a plot of the Hall coefficient of InAs samples. InAs is a semiconducting compound.

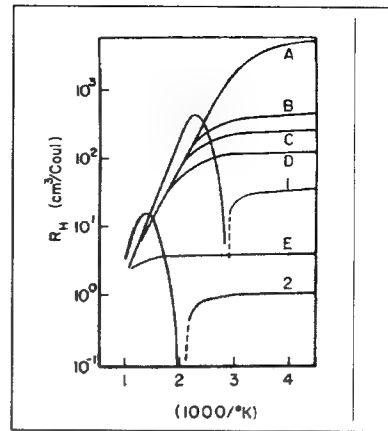


Figure 15. Hall coefficient vs. reciprocal temperature for InAs²⁷.

Using $R_H = 1/nq$, the corresponding Hall coefficient (R_H) for $n = 4.0 \times 10^{18} \text{ e}^-/\text{cc}$ is $1.56 \text{ cm}^3/\text{Coul}$ and for $n = 1.25 \times 10^{18} \text{ e}^-/\text{cc}$ is $5.0 \text{ cm}^3/\text{Coul}$.

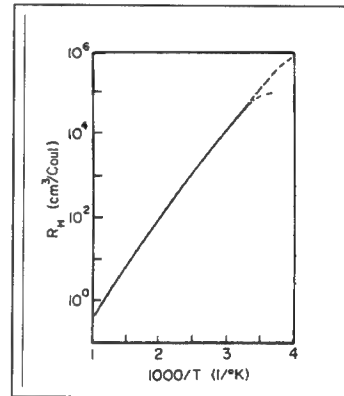


Figure 16. Hall coefficient versus reciprocal temperature curve for intrinsic germanium²⁶.

Figure 16 shows the Hall coefficient curve for intrinsic germanium. Notice how this is about 3 thousand times higher than WO_3 in the same temperature range.

3.2.5. Hall Mobility of WO₃ Above Room Temperature

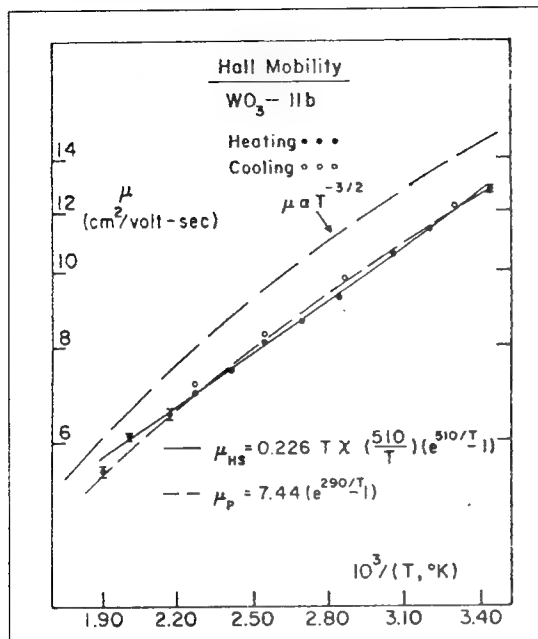


Figure 17. Hall mobility versus reciprocal temperature for a WO₃ crystal above room temperature²⁶.

The Hall mobility $\mu_H = R_H \sigma$ is usually the same as the drift mobility²⁸. Figure 17 shows how μ_H increases as T decreases. This is characteristic of electrons in interaction with lattice vibrations. The value of μ_H is small, which means lower energy acoustic phonons are probably not coupling to the electrons. The upper curve shows the $T^{-3/2}$ power dependence for acoustic modes, which does not fit the data. The 2 lower curves are optical mode scattering models. The μ_{HS} curve is the Howarth-Sondheimer²⁹ perturbation model, while the μ_P curve is the large polaron intermediate coupling theory of Lee, Low and Pines³⁰. These show a better fit to scattering by optical modes.

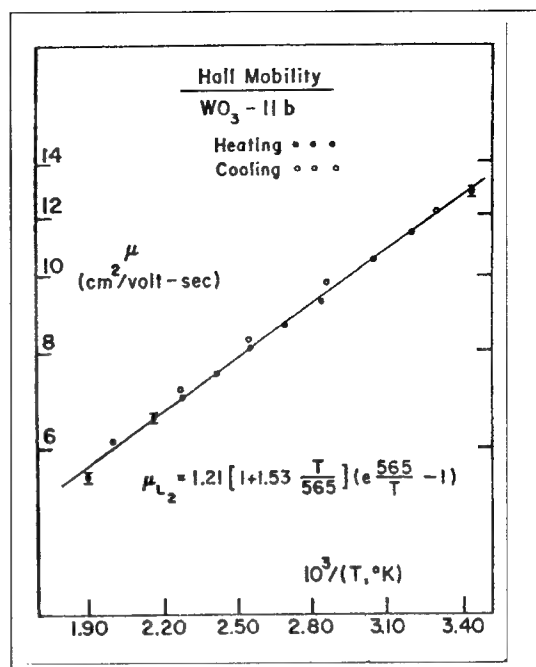


Figure 18. Hall mobility vs. reciprocal temperature for a WO₃ crystal below room temperature²⁶.

Figure 18 shows a fit to the Langreth³¹ theory of large polaron mobility at finite temperature.

In both figures 17 and 18, the mobility is greater than unity, a necessary condition for the formation of a large polaron band²⁶.

3.2.6. Small and Large Polarons

A polaron is the result of the electron lowering its own energy to polarize the surrounding lattice, as is seen in part (c) of figure 9. This lowering of energy acts to trap the electron in the local distortion it creates around a given lattice site³². The polaron can also be thought of as an electron surrounded by a stress field.

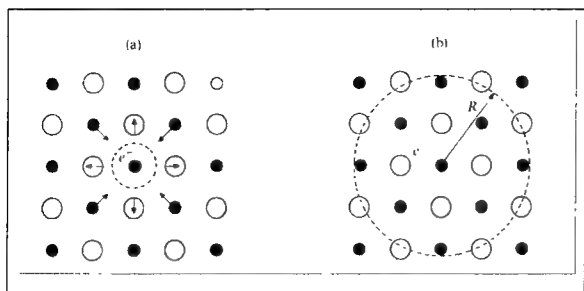


Figure 19. Small (a) and large (b) polarons³¹.

The polaron radius, r_p , can be approximated using⁶ $r_p = \hbar(2m^*k\theta_l)^{-1/2}$ where θ_l is the characteristic temperature of the longitudinal optical modes and m^* is the effective mass. In WO_3 , the effective mass is 1.4 times the rest mass. The resulting polaron radius is about 8.5 angstrom. The separation between tungsten atoms is 3.8 angstrom. This means the polaron is a large polaron. These large polarons have enough overlap to allow some conduction.

3.2.7. Conductivity of M_xWO_3 (Tungsten Bronzes)

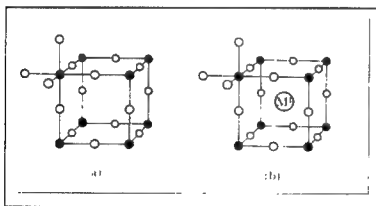


Figure 20. (a) ReO_3 structure; (b) Perovskite-like tungsten bronze structure. Filled circles are W^{6+} , open circles are O^{2-} , M^I is a metal ion³³.

WO_3 has a distorted version of the ReO_3 structure (figure 20a), which is a simple cubic lattice of tungsten with each tungsten atom the center of a WO_6 octahedron. Figure 21 shows a more accurate representation of the WO_3 structure.

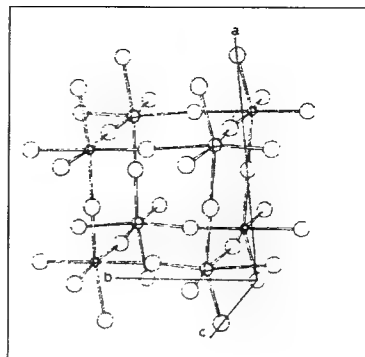


Figure 21. WO_3 structure³⁴.

When small amounts of metals (M), usually hydrogen or sodium, are added to WO_3 , a tungsten bronze is formed. The WO_3 lattice restructures with a proton or a positive metal ion in the center of the simple cubic tungsten lattice (figure 20b). In tungsten bronzes, metal atoms donate their electrons to the empty conduction band of the host WO_3 lattice. These extra electrons lead to a semiconducting or a metallic state, depending on x .

Figure 22 illustrates this for H_xWO_3 . The curves for low x show low conductivity which increases with temperature. The curve for $x = 0.32$ shows better conductivity which is independent of temperature below about 20 K. This is metallic behavior. As x decreases, the bandwidth decreases until the polarization energy is large compared to bandwidth, which is the necessary condition for the formation of a small polaron. The solid lines for small x are fits to a variable range hopping model³⁵ with $T^{-1/4}$ temperature dependence.

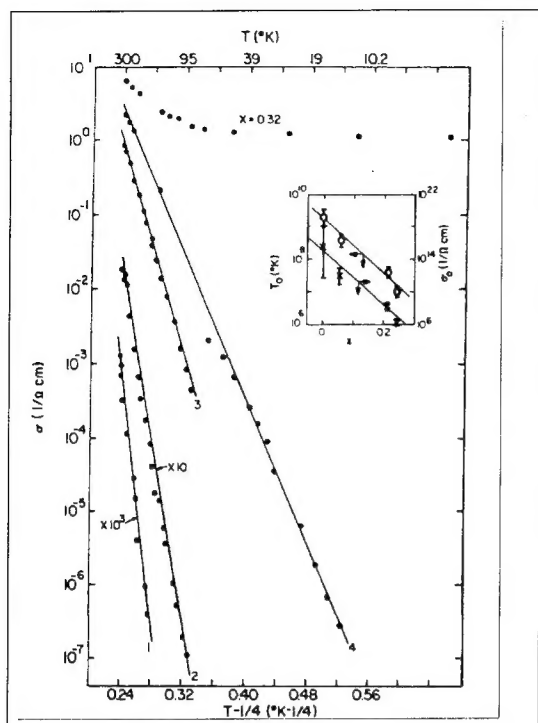


Figure 22. Logarithm of conductivity vs. $T^{-1/4}$ for amorphous H_xWO_3 films at 5 different x values. Curve 1 has $x = 0$, curve 2 has $x = 0.06$, curve 3 has $x = 0.21$ and curve 4 has $x = 0.24$ ³⁶.

Figure 19a shows a small polaron. Small polarons do not overlap enough for conduction. These localized electrons cannot move unless they are bumped by a thermal lattice phonon into an adjoining site. This type of conduction is called hopping conduction.

In Na_xWO_3 , sodium tungsten bronze, the lattice restructures with an Na^+ ion in the center of the simple cubic tungsten lattice. Na_xWO_3 turns metallic at about $x = 0.25$, but this is dependent on preparation³⁷.

The temperature dependence of the Hall carrier concentration at $x = 0.23$ in figure 23 suggests localization of the carriers³⁹.

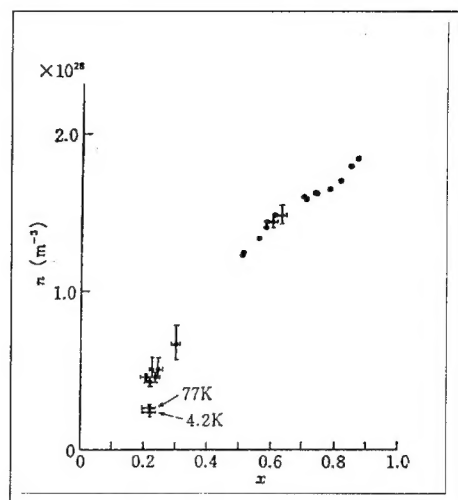


Figure 23. Hall carrier density of Na_xWO_3 versus Na concentration³⁸.

In figure 24, all values of x exhibit metallic behavior.

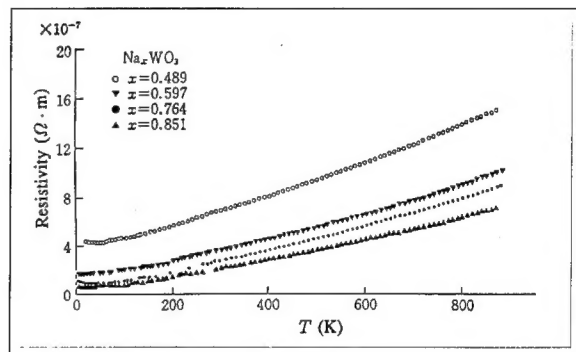


Figure 24. Resistivity of Na_xWO_3 vs. temperature for varying x values³⁹.

3.2.8. Shear Planes in Substoichiometric WO_3

When WO_3 is heated in vacuum, oxygen and water are driven off, and the material becomes substoichiometric WO_{3-x} with x being a small number.

As illustrated in figure 25, when WO_3 is being heated, oxygen vacancies preferentially form discs and then planes. These planes are called antiphase boundaries. When there is enough energy in the lattice, the lattice shears along

the plane of vacancies, removing the vacancies. This is called crystallographic shear.

Crystallographic Shear (CS) or Magnelli phases are quasistable. In WO_3 they are of the form $\text{M}_n\text{O}_{3n-1}$. They include $\text{W}_{20}\text{O}_{58}$, $\text{W}_{40}\text{O}_{118}$ and $\text{W}_{50}\text{O}_{148}$.

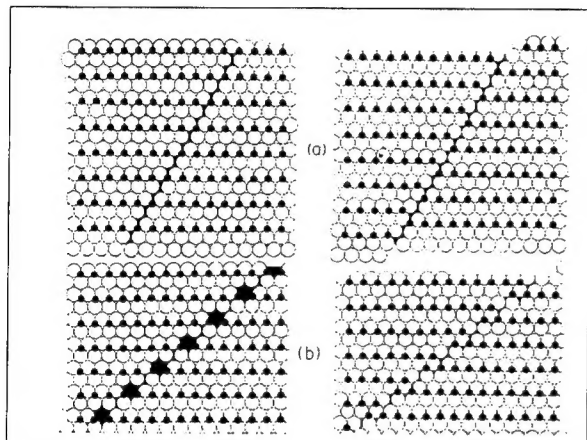


Figure 25. Antiphase boundary (on left) and crystallographic shear (on right) along 2 different crystallographic directions⁴⁰.

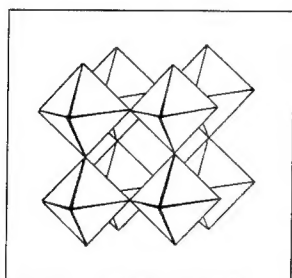


Figure 26. MO_6 octahedra stacking⁴¹.

Another effect occurs with crystallographic shear. Before shearing, the WO_6 octahedra share corners, as is shown in figure 26. After shearing, some or all neighboring octahedra along the CS plane share edges, as shown in figure 27. This results in removing some oxygen atoms.

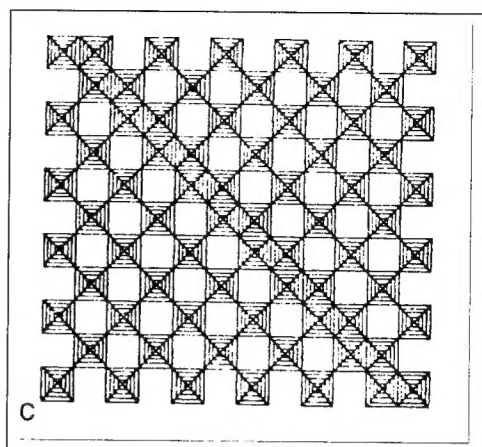


Figure 27. A $\{101\}$ shear plane in WO_3 . Shaded areas are WO_6 octahedra as viewed from above⁴².

A comparison of figure 11 to figure 28 shows that removal of oxygen decreases the resistivity. This can be explained by the changes in carrier concentration in the material.

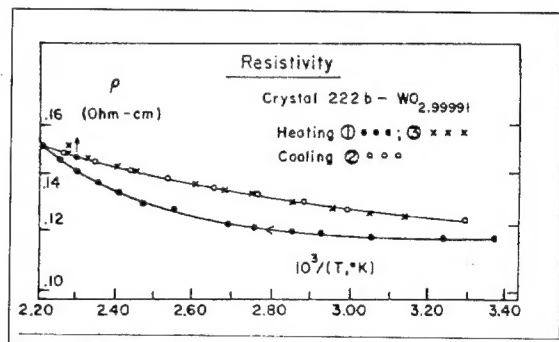


Figure 28. Resistivity vs. $1/T$ for a single crystal having ratio of 2.99991²⁶.

Figure 29 shows an increase in the carrier concentration. This can be explained by the observation that there is a different conduction process occurring through the CS planes, which were observed to cross and separate the yellow stoichiometric WO_3 regions. Since these planes are comparatively lower in oxygen defects after shearing, there should be less scattering of electrons traveling through these planes. An initial irreproducible decrease in the carrier concentration is observed, which can be explained by the alignment of oxygen

vacancies in the formation of antiphase boundaries.

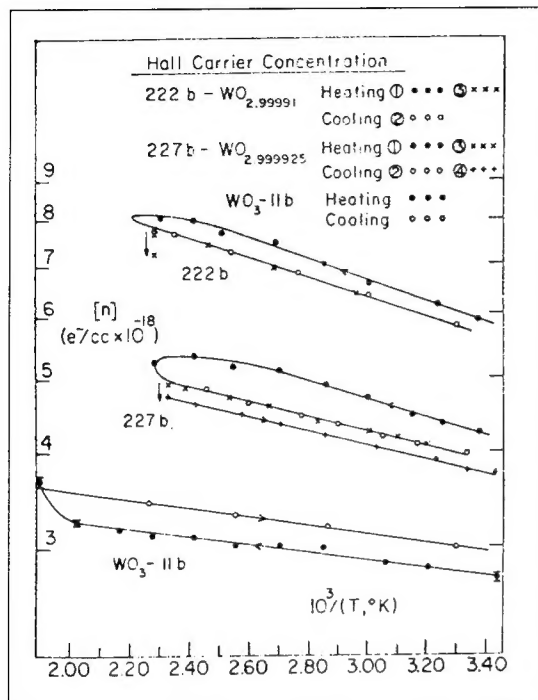


Figure 29. Hall carrier concentration vs. $1/T$ for a 2 single crystals having O/W ratios of 2.99991 and 2.999925 compared with stoichiometric WO_3 ²⁶.

3.3. Conclusions

Study of the differences in conductivity of the various forms of WO_3 show that there is enough difference to begin an effort to use photochromic WO_3 to produce an optically addressed, electronically read memory.

3.4. Future Plans for Page Memory

We should begin our page memory readout system using the following plan:

3.4.1. Thin Film Production

We should fabricate thin films of WO_3 on quartz and silicon substrates. The National Nanofabrication Facility (NNF) would be ideal for this.

3.4.2. Resistance Measurements

We should then measure the change in oxide resistance of the thin film with change in state from yellow to blue.

3.4.3. Memory Element Design

If the measured resistance difference is large, we should design a diode memory with each individual diode being a piece of our new media. If the measured resistance difference is small, we should design a flip flop such that the measured resistance change will cause a change in the flip flop's state. Design should be integrable and capable of as much size reduction as possible.

3.4.4. Memory Element Test

We should then fabricate and test the page memory.

- ²⁵Cox, P.A., *Transition Metal Oxides*, p. 48, Clarendon Press, Oxford, 1992.
- ²⁶Berak, J. & Sienko, M., *Journ. Solid State Chem.* **2**, 109-133 (1970).
- ²⁷Folberth, O.G., *et al.*, *Z. Naturf.* **9a**, 954 (1954) as quoted in Schröder, K., *Electronic, Magnetic, and Thermal Properties of Solid Materials*, p. 423, Marcel Dekker, 1978.
- ²⁸Schröder, K., *Electronic, Magnetic, and Thermal Properties of Solid Materials*, p. 414, Marcel Dekker, 1978.
- ²⁹Howarth, D. and Sondheimer, E., *Proc. Roy. Soc. London* **A219**, 53 (1953).
- ³⁰Lee, T.D., Low, F.E. and Pines, D., *Phys. Rev.* **90**, 297 (1953); Low, F.E., and Pines, D., *Phys. Rev.* **91**, 193 (1953).
- ³¹Langreth, D.C., *Phys. Rev.* **159**, 717 (1967).
- ³²Cox, P.A., *The Electronic Structure and Chemistry of Solids*, p. 180, Oxford, 1987.
- ³³Duffy, J.A., *Bonding, Energy Levels and Bands in Inorganic Solids*, p. 185, Longman, 1990.
- ³⁴Salje, E., *Acta Cryst.*, **B33**, 574-577, (1977)
- ³⁵Ambegaokar, V., *et al.*, *Phys. Rev. B* **4**, 2612 (1971).
- ³⁶Crandall, R. & Faughman, B., *Phys. Rev. Lett.* **39**, 232-235 (1977)
- ³⁷Muhlestein, L.D., and Danielson, G.C., *Phys. Rev.* **158**, 825 (1967).
- ³⁸Lightsey, P.A., *Phys. Rev. B* **14**, 4730 (1976) as quoted in Tsuda, N. *et al.*, eds., *Electronic Conduction in Oxides*, p. 146, Springer-Verlag, 1990.
- ³⁹Ellerbeck, L. *et al.*, *J. Chem. Phys.* **35**, 298 (1961).
- ⁴⁰Eyring, L. and Tai, L., *The Structural Chemistry of Some Complex Oxides*, in Hannay, N.B., *Treatise on Solid State Chemistry Vol. 3*, Plenum, 1976.
- ⁴¹Cox, P.A., *Transition Metal Oxides*, p. 22, Clarendon Press, Oxford, 1992.
- ⁴²Iguchi, E. and Tilley, R.J.D., *Journ. Solid State Chem.* **21**, 49-56 (1977).